Proceedings of the ASME 2020 Dynamic Systems and Control Conference
DSCC 2020
October 4-7, 2020, Pittsburgh, Pennsylvania, USA

DSCC2020-3289

IONIC POLYMER METAL COMPOSITE SENSORS WITH ENGINEERED INTERFACES (EIPMCS): COMPRESSION SENSING MODELING AND EXPERIMENTS

Rebecca Histed[1], Justin Ngo[2], Omar A. Hussain[2], Chantel Lapins[2], Kam K. Leang[2], Yiliang Liao[1], Matteo Aureli[1,*]
[1]Department of Mechanical Engineering, University of Nevada, Reno
1664 N Virginia St., Reno, Nevada 89557-0312
[2]Department of Mechanical Engineering, University of Utah
1495 E. 100 S., Salt Lake City, Utah 84112

ABSTRACT

In this paper, we examine the development of tailored 3D-structured (engineered) polymer-metal interfaces to create enhanced ionic polymer-metal composite (eIPMC) sensors towards soft, self-powered, high sensitivity strain sensor applications. First, a physics-based chemoelectromechanical model is developed to predict the sensor behavior of eIPMCs by incorporating structure microfeature effects in the mechanical response of the material. The model incorporates electrode surface properties, such as microscale feature thickness, size and spacing, to help define the mechanical response and transport characteristics of the polymer-electrode interface. Second, two novel approaches are described to create functional samples of eIPMC sensors using fused deposition manufacturing and inkjet printing technologies. Sample eIPMC sensors are fabricated for experimental characterization. Finally, experimental results are provided to show superior performance in the sensing capabilities compared to traditional sensors fabricated from sheet-form material. The results also validate important predictive aspects of the proposed minimal model.

INTRODUCTION

Ionic polymer metal composites (IPMCs) are smart electroactive soft composite materials that comprise a thin electrically charged polymer membrane, plated with noble metal electrodes, and infused with a charged solution [1–4]. By combining self-powered sensor behavior and soft mechanical characteristics, IPMCs emerge as an ideal candidate for soft strain sensor applications in bioengineering, rehabilitation and medicine, soft robotics, and human-machine interactions. However, long-standing challenges of limited sensitivity, poor property control, and non-versatile mode of operation have so far dramatically limited the use of IPMCs in critical engineering applications. From a fundamental perspective, these challenges can be traced back to inconsistent and uncontrollable morphology of IPMC polymer-metal interfaces, resulting from poor controllability of traditional IPMC fabrication processes. It is therefore hypothesized that the multiphysics sensing properties of IPMCs can be dramatically enhanced by tailored 3D-structured ("*engineered*") polymer-metal interfaces. To test this hypothesis, in this paper, we propose to use a recently-developed IPMC 3D-printing fabrication process [5] and inkjet printing to create IPMCs with engineered interfaces and then develop a model that captures the structure-property relationships to demonstrate enhanced strain sensing performance. Thus, the contribution of this paper is a new class of *engineered* IPMCs (eIPMCs) with superior multiphysics properties towards soft, self-powered, high sensitivity strain sensor applications.

Recent research efforts have emphasized the critical need for soft strain sensors for a variety of applications, spanning from bioengineering, rehabilitation and medicine, soft robotics, to human-machine interactions [6, 7]. Despite desirable soft mechanical characteristics, current soft strain sensors often suffer from the major drawback of necessitating externally powered electric circuits, which convert the strain-induced changes of electrical impedance of the sensor into usable electrical signals. This severely limits the possibility to make such sensors light weight, comfortable to wear, and capable of functioning over long periods of time. On the other hand, existing self-powered sensors, for example piezoelectric ceramics, are typically very stiff, non-stretchable, and limited to extremely small deformations [8]. Thus, there is a clear and urgent need to identify

*Address all correspondence to this author; maureli@unr.edu.

novel material systems that combine self-powered behavior with soft mechanical characteristics for creating next generation strain sensors.

Ionic polymer metal composites have the strong potential to address the above mentioned need by qualifying as promising candidates for self-powered soft strain sensors. In the sensing mode, when mechanical deformation is imposed on an IPMC strip, redistribution of the mobile ions within the membrane results in an electrical signal at the IPMC electrodes [9]. The concept of IPMC sensors is extremely attractive because of their soft nature (effective Young's modulus [10] of the order of 100 MPa), their excellent linearity with respect to imposed mechanical deformations [9], and their self-powered operation (IPMC sensors do not require batteries or external energy sources). However, comparatively fewer studies have focused on the feasibility of IPMCs as force and displacement sensors [11–14] and energy harvesting systems [10, 15–17]. In addition, most of the applications have concentrated on bending mode systems.

The long-standing challenges of limited sensitivity [12], poor property control, and non-versatile mode of operation have so far dramatically hampered the use of IPMC sensors. Specifically, IPMCs exhibit extremely large variability in terms of their multiphysics properties (in particular, capacitance [18]). This variability and inconsistency, in turn, demand extensive property and performance characterization of each individual IPMC sample before use in any sensor system. In addition, until very recently [19–22], the limited understanding of the fundamental nature of material response to non-bending deformation in IPMCs has effectively precluded major breakthroughs in the development of non-bending mode sensors. In particular, a theoretical explanation of the compression sensing mode (electrical transduction of deformation in the thickness direction due to applied pressure normal to the electrodes) was only offered in 2017 in [22] and therein attributed to inhomogeneous strain through the IPMC thickness. Since the inhomogeneous deformation depends on material properties that cannot be controlled by design during the fabrication process, traditional IPMC sensitivity in compression mode is typically very low (e.g. 3 μA per 1% strain deformation [22]). Therefore, this very attractive sensing mode has not been well explored, and from a fundamental perspective, all these challenges can be traced back to inconsistent and uncontrollable morphology of IPMC polymer-metal interfaces, resulting from poor controllability of traditional fabrication processes.

This paper tackles the challenge of dramatically improving the multiphysics properties of IPMCs by engineering the role of polymer-metal interface in defining the material response. Novel eIPMC test samples are fabricated using 3D-printing the inkjet technology to create sensors, and modeling and experimental results are presented to demonstrate enhanced performance.

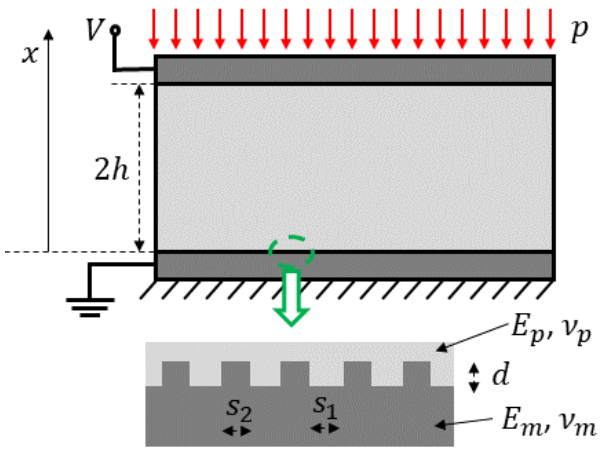

FIGURE 1. Schematic representation and nomenclature of the problem, with detail of the engineered interface region. In the figure, V is the electric potential at the movable electrode, p is the applied pressure, h is the polymer semithickness, x is the through-the-thickness coordinate. Young's modulus and Poisson's ratio are E_p, ν_p for the polymer and E_m, ν_m for the metal electrodes. Geometry of the engineered interface is described by feature size s_2, spacing s_1 and height d.

MODELING

Problem statement and nomenclature

The problem under consideration is schematically depicted in Fig. 1, along with the relevant nomenclature. We study the chemoelectromechanical response via a purely one-dimensional through-the-thickness problem for an eIPMC of semithickness h with its grounded engineered electrode at $x = 0$ and its movable bare electrode at $x = 2h$. For generality, the two-dimensional pattern in the interface of the engineered electrode is assumed to be fabricated with given dimensions as shown in Fig. 1, and it could represent ridges in the direction orthogonal to the page or pillar-like cylindrical structures arranged in the plane $x = 0$ of the electrode. As explained later, we will forego a detailed description of the interface and will assume that the polymer-metal interface is sharp and located at $x = 0$. Young's modulus and Poisson's ratio of the material are indicated with E and ν, respectively, with a subscript p or m to indicate polymer or metal, respectively. The polymer is assumed to be mechanically and electrochemically homogeneous and isotropic. We will consistently neglect the presence of steric effects [23], composite layers [24], and electrode surface roughness [18, 25]. We will also assume that the electrodes are perfectly rigid and conductive.

A minimal mechanical model

We consider a purely one-dimensional plane strain compression model, upon quasi-static application of a possibly time-varying uniform pressure $p(t)$ normal to the movable electrode initially at $x = 2h$. Far from the engineered electrode at $x = 0$, the engineering stress field in the material is uniform and given by $-p$ while the engineering strain is given by $\varepsilon_x = -p/E_p$ (and,

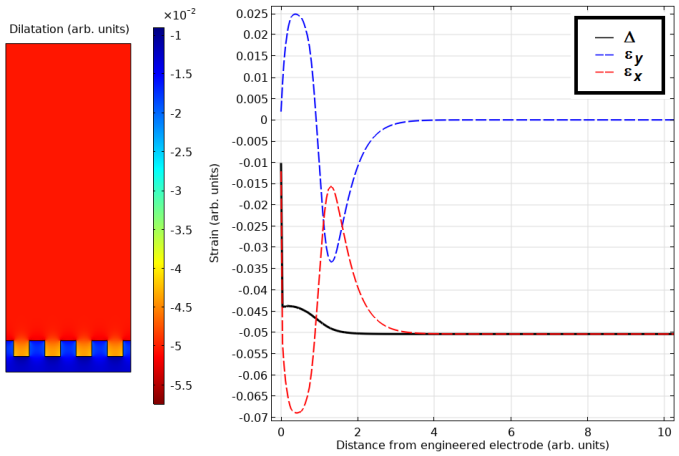

FIGURE 2. Representative finite element results on the dilatation Δ in a section of the eIPMC subject to uniaxial compression in the x-direction, along with strain profiles for ε_x and ε_y.

obviously, $\varepsilon_y = 0$). In the vicinity of the engineered electrode, the strain field becomes significantly more complicated due to stress concentration effects and the complicated geometric pattern on the engineered electrode. This inhomogeneous strain developed in the eIPMC is responsible for the sensing behavior.

In order to capture the inhomogeneous deformation that develops in the eIPMC upon application of a mechanical compression, rather than formalizing an accurate homogenization procedure for the micromechanical properties of the engineered electrode, for example along the lines of [26], we conduct a representative finite element simulation on a simplified model to understand fundamental properties of the strain field, see Fig. 2. In the representative simulation, we assume linear, homogeneous, isotropic elastic behavior for metal and polymer, we set $E_m = 50E_p$, $\nu_m = 0.3$, and $\nu_p = 0.49$, and we design a simple periodic pattern for the protrusion of the engineered electrode, with $s_1 = s_2 = d$. The hypothesis of linear, homogeneous, isotropic elastic behavior for IPMC material is common in the literature [10, 22]. We run a linear static plane strain analysis on a representative section of eIPMC and we determine the dilatation field $\Delta = \varepsilon_x + \varepsilon_y$ (or trace of the strain tensor), that is, the local relative change in volume of the polymer upon mechanical compression [10]. As expected, simulations show that, far from the engineered electrode, the dilatation is simply equal to the bulk value $\Delta = \varepsilon_x = -p/E_p$. In the vicinity of the engineered electrode, on the other hand, the strain field becomes two dimensional ($\varepsilon_y \neq 0$). The absolute value of the dilatation decreases over a lengthscale d (which can be presumed of the same order of the height of the protrusions in the electrode pattern) to a value at the electrode $x = 0$, whose exact magnitude depends in a complicated way on material and geometric properties of the interface. We will assume that this peculiar behavior of the dilatation can be sufficiently well described, in a simplified one-dimensional analysis, by the following model

$$\Delta(x,t) = -\frac{p(t)/E_p}{[1 + B\exp(-x/d)]}, \tag{1}$$

where B takes on the role of a tuning parameter, in the absence of a more detailed micromechanical homogenization which is outside the scope of this paper. As explained later, the detailed form of Eq. (1) has only limited impact on the description of the sensing behavior, so we consider the simple representation offered above. It is, however, important to note that B represents a measure of the asymmetry in the mechanical behavior of the regions in proximity of the engineered electrode and the bare electrode. Specifically, if both electrodes were bare and nominally identical, $B = 0$.

Note that this derivation has been obtained independently of possible chemoelectromechanical coupling, effectively separating the problem at hand in two simpler substeps, the first of which is determining the mechanical deformation in response to a pressure input. We will use this local dilatation in the next substep, where the imposed mechanical deformation will be correlated to the chemoelectromechanical response of the eIPMC.

Linear chemoelectromechanical sensing

Herein, we will focus on the linear response of the eIPMC compression sensor, under the hypothesis of small: deformations, electric potentials, and deviations of the counterion concentration with respect to the concentration at rest. The governing equations for IPMC chemoelectromechanical sensing behavior in the nonlinear case have been developed in [9], and further enriched in [22, 27]. With specialization to the case at hand, and following in part [28], a linearized version of the equations in [9] is given by

$$-\varepsilon_0\varepsilon_r \frac{\partial^2 \psi(x,t)}{\partial x^2} = F\left(c(x,t) - c_0[1 - \Delta(x,t)]\right), \tag{2a}$$

$$\frac{\partial c(x,t)}{\partial t} + c_0 \frac{\partial \Delta(x,t)}{\partial t} = D\left[\frac{\partial^2 c(x,t)}{\partial x^2} + \frac{F c_0}{RT}\frac{\partial^2 \psi(x,t)}{\partial x^2}\right]. \tag{2b}$$

Equation (2a), consistent with the model in [10], is Poisson's equation, which establishes the relationship (Gauss' law) between the electric potential ψ and the free charge in the eIPMC, where F is Faraday's constant, c is the concentration of mobile counterions, c_0 is the concentration of fixed ions, and ε_0 and ε_r are the vacuum permittivity and the eIPMC relative permittivity, respectively, and assumed to be constant. It is important to note that the concentrations of mobile counterions and fixed ions are calculated with respect to the deformed volume of the eIPMC. Equation (2b) is the linearized generalized Nernst-Planck equation which establishes conservation of charge in the eIPMC. Here, D is the counterion diffusivity in the bulk polymer, R is the universal gas constant, and T is the IPMC temperature. Note that, when compared to the model reported in [10],

Eq. (2b) is enriched with the important advective term $c_0\partial\Delta/\partial t$, see also [28], to capture the change in concentration, even in the absence of ion flux, due to the mechanical deformation of the eIPMC. The right hand side of Eq. (2b) is also recognized as the (negative) divergence of the linearized ion flux J which is defined as $J=-D[\partial c/\partial x+(Fc_0)/(RT)\partial\psi/\partial x]$.

The governing equations are subject to appropriate boundary and initial conditions. We set here initial chemoelectromechanically neutral conditions as $p(0)=0$, $\psi(x,0)=0$, and $c(x,0)=c_0$. Boundary conditions are such that $\psi(0)=0$ at the grounded electrode and $\psi(2h)=V$ at the movable electrode. The value of V will be prescribed later in the study of short-circuit (SC) or open-circuit (OC) conditions. In addition, as customary, we prescribe ion-blocking conditions at the electrodes at $x=0$ and $x=2h$, which set the ion flux to zero at the polymer-electrode interfaces, that is, $J(0)=J(2h)=0$ [28].

As in standard practice, it is convenient to nondimensionalize the governing equations and their boundary conditions by scaling all lengths and displacements with the polymer semithickness h, the time variable t with a characteristic time t_0 to be defined in the following, the electric potential ψ with the thermal voltage $V_{\rm th}=RT/F$. In addition, it is useful to nondimensionalize the applied pressure p with the bulk Young's modulus of the polymer E_p, so that $p/E_p=\tilde{p}$, where the superimposed tilde notation indicates a nondimensional quantity. Thus, the dilatation becomes $\Delta(\tilde{x},\tilde{t})=-\tilde{p}(\tilde{t})/K(\tilde{x})$, with $K(\tilde{x})=1+B\exp(-\tilde{x}/\tilde{d})$. We also define the nondimensional counterion over-concentration $\tilde{\chi}(\tilde{x},\tilde{t})=[c(\tilde{x},\tilde{t})-c_0]/c_0$. With these positions, and neglecting the explicit dependence on the independent variables, the nondimensional form of Eqs. (2) reads

$$-\delta^2\frac{\partial^2\tilde{\psi}}{\partial\tilde{x}^2}=\tilde{\chi}-\tilde{p}/K, \tag{3a}$$

$$\frac{\partial\tilde{\chi}}{\partial\tilde{t}}-\frac{\partial\tilde{p}/K}{\partial\tilde{t}}=\delta\left[\frac{\partial^2\tilde{\chi}}{\partial\tilde{x}^2}+\frac{\partial^2\tilde{\psi}}{\partial\tilde{x}}\right], \tag{3b}$$

where we have also defined $\delta=\lambda_D/h$ as the ratio between the Debye screening length $\lambda_D=\sqrt{(\varepsilon_0\varepsilon_r RT)/(F^2c_0)}$ and the polymer semithickness h and the characteristic time $t_0=\lambda_D^2/D$ is selected as the diffusion timescale within the charge boundary layers. Similarly, nondimensional boundary conditions are $\tilde{\psi}(0)=0$, $\tilde{\psi}(2)=\tilde{V}$, with $\tilde{V}=V/V_{\rm th}$, and $\tilde{J}(0)=\tilde{J}(2)=0$. Note that the form of the presented equations and boundary conditions is slightly different from that used in [22], as the concentrations therein are expressed per unit undeformed volume.

It is important to note that, in practical IPMC and eIPMC applications, $\lambda_D\approx10^{-10}$ m and the parameter δ is thus of the order of 10^{-6} [29]. Therefore, Eqs. (3) describe a singularly perturbed system whose solution is best attacked by way of matched asymptotic expansions [30]. We will sketch below the solution procedure, which follows the steps in [22, 29]. In what follows, we will drop the superscript tilde for notational convenience although we will consistently refer to nondimensional variables, except where explicitly noted. We will also use a superimposed dot notation to indicate time derivatives and a prime notation to indicate spatial derivatives.

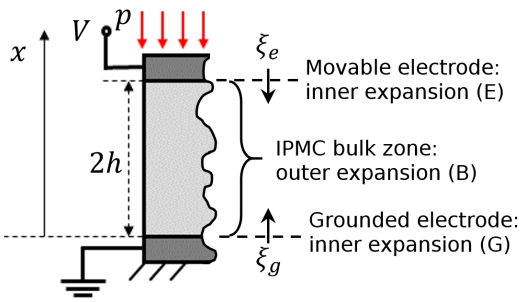

FIGURE 3. Schematic representation of the strategy of matched asymptotic expansions, with labels indicating the three expansion zones.

Matched asymptotic expansions

The problem is attacked by the technique of matched asymptotic expansions. We will consider a bulk zone for which an outer expansion is sought, and two boundary layer zones, in proximity of the polymer-metal interfaces, where an inner expansion is sought. The idea is sketched in Fig. 3 and the relevant governing equations are developed in the next subsections.

Outer expansion: In the eIPMC bulk, we consider a regular asymptotic expansion of χ and ψ in terms of the small parameter δ, such that $\chi^{(B)}=\chi_0^{(B)}+\delta\chi_1^{(B)}+\delta^2\chi_2^{(B)}+\dots$ and $\psi^{(B)}=\psi_0^{(B)}+\delta\psi_1^{(B)}+\delta^2\psi_2^{(B)}+\dots$, where the symbol (B) indicates the outer expansion in the bulk. Substituting these representations in Eqs. (3), and approximating the outer solution with its leading order term of $\mathcal{O}(\delta^0)$, we obtain

$$\chi^{(B)}=\chi_0^{(B)}=p/K(x), \tag{4a}$$

$$\psi^{(B)}=\psi_0^{(B)}=-p/K(x)+A_1^{(B)}(t)x+A_0^{(B)}(t), \tag{4b}$$

where $A_1^{(B)}(t)$ and $A_0^{(B)}(t)$ are yet unknown functions of time.

Inner expansion at the grounded electrode: In the vicinity of the grounded electrode at $x=0$, we magnify the spatial coordinate by introducing the stretched variable $\xi_g=x/\delta$, where the subscript g stands for grounded electrode. We perform the change of variables in Eq. (3) and seek a regular asymptotic expansion of χ and ψ in the boundary layer region in terms of the small parameter δ, such that $\chi^{(G)}=\chi_0^{(G)}+\delta\chi_1^{(G)}+\delta^2\chi_2^{(G)}+\dots$ and $\psi^{(G)}=\psi_0^{(G)}+\delta\psi_1^{(G)}+\delta^2\psi_2^{(G)}+\dots$, where the symbol (G) indicates the inner expansion in the boundary layer at the grounded electrode. Thus, at the leading order, Eqs. (3) reduce to $\chi_0^{(G)}+(\psi_0^{(G)})''=p/K(0)$ and $(\chi_0^{(G)}+\psi_0^{(G)})''=0$, and by approximating $\chi^{(G)}$ and $\psi^{(G)}$ with their $\mathcal{O}(\delta^0)$ terms, we obtain

$$\chi^{(G)} = p/K(0) + C_2^{(G)}(t)\mathrm{e}^{-\xi_g}, \tag{5a}$$

$$\psi^{(G)} = -p/K(0) - C_2^{(G)}(t)\mathrm{e}^{-\xi_g} + A_0^{(G)}(t), \tag{5b}$$

where $A_0^{(G)}(t)$ and $C_2^{(G)}(t)$ are yet unknown functions of time. In the derivation of Eqs. (5) we have also used the fact that these solutions must be bounded at $\xi_g \to \infty$, thus effectively determining the null values of integration constants of the solution diverging terms $C_1^{(G)}(t)\mathrm{e}^{\xi_g}$ and $A_1^{(G)}(t)\xi_g$.

Inner expansion at the movable electrode: In the vicinity of the movable electrode at $x = 2$, we magnify the spatial coordinate by introducing the stretched variable $\xi_e = (2-x)/\delta$, where the subscript e stands for movable electrode. We perform the change of variables in Eq. (3) and seek a regular asymptotic expansion of χ and ψ in the boundary layer region in terms of the small parameter δ, such that $\chi^{(E)} = \chi_0^{(E)} + \delta\chi_1^{(E)} + \delta^2\chi_2^{(E)} + \dots$ and $\psi^{(E)} = \psi_0^{(E)} + \delta\psi_1^{(E)} + \delta^2\psi_2^{(E)} + \dots$, where the symbol (E) indicates the inner expansion in the boundary layer at the movable electrode. By closely following the steps above, we obtain

$$\chi^{(E)} = p/K(2) + C_2^{(E)}(t)\mathrm{e}^{-\xi_e}, \tag{6a}$$

$$\psi^{(E)} = -p/K(2) - C_2^{(E)}(t)\mathrm{e}^{-\xi_e} + A_0^{(E)}(t), \tag{6b}$$

where $A_0^{(E)}(t)$ and $C_2^{(E)}(t)$ are yet unknown functions of time and, as above, we have enforced boundedness of solutions at $\xi_e \to \infty$.

Matching: The inner and outer expansions determined above must be matched in such a way they share a common limit in their overlap regions so that, in particular, $\lim_{x\to 0}\psi^{(B)} = \lim_{\xi_g\to\infty}\psi^{(G)}$ and $\lim_{x\to 2}\psi^{(B)} = \lim_{\xi_e\to\infty}\psi^{(E)}$, and similarly for the over-concentration solutions. These conditions yield immediately $A_0^{(B)}(t) = A_0^{(G)}(t)$ and $A_0^{(B)}(t) + 2A_1^{(B)}(t) = A_0^{(E)}(t)$.

The next matching condition pertains to continuity of the ion flux and can be enforced through the process devised in [29]. Summarizing the procedure, by integrating Eq. (3b) from the electrode to an arbitrary location in the polymer bulk, enforcing the ion-blocking condition at the interface, specializing the left-hand side to the inner solution and the right-hand side to the outer solution, and considering only the leading order of the solution, the matching yields

$$\dot{C}_2^{(G)}(t) = A_1^{(B)} = -\dot{C}_2^{(E)}(t). \tag{7}$$

Finally, the last matching condition stems from enforcing the voltage boundary conditions at the electrodes on the inner solutions. These are

$$\psi^{(G)}(\xi_g = 0) = -p/K(0) - C_2^{(G)}(t) + A_0^{(G)}(t) = 0, \tag{8a}$$

$$\psi^{(E)}(\xi_e = 0) = -p/K(2) - C_2^{(E)}(t) + A_0^{(E)}(t) = V. \tag{8b}$$

We combine together the matching conditions and Eqs. (8), and we take a Laplace transform of Eq. (7), using a hat to indicate transformed quantities and s as the Laplace variable. Then, we obtain the following linear system for $\hat{A}_1^{(B)}$ and $\hat{A}_0^{(B)}$

$$\begin{cases} (-s^{-1})\hat{A}_1^{(B)} + \hat{A}_0^{(B)} = p/K(0) \\ (2+s^{-1})\hat{A}_1^{(B)} + \hat{A}_0^{(B)} = p/K(2) + V \end{cases} \tag{9}$$

Solution of the linear system completes the determination of the unknown integration constants $\hat{A}_1^{(B)}$ and $\hat{A}_0^{(B)}$, that is,

$$\hat{A}_1^{(B)} = \frac{s}{2(s+1)}\hat{V} + \frac{s[1/K(2) - 1/K(0)]}{2(s+1)}\hat{p}, \tag{10a}$$

$$\hat{A}_0^{(B)} = \frac{1}{2(s+1)}\hat{V} + \frac{K(0) + K(2)[1+2s]}{2K(0)K(2)(s+1)}\hat{p}, \tag{10b}$$

from which the other constants can be directly determined, if desired. For ease of notation, we denote with $\gamma = [1/K(2) - 1/K(0)]$ which represents a measure of the asymmetry of the mechanical properties of the eIPMC in the vicinity of the grounded electrode (the engineered electrode) and the movable electrode (the bare electrode). In particular, $0 \le \gamma \le 1$ and note that, if the two interfacial regions are nominally identical with no asymmetry, then $\gamma = 0$ and the term $\hat{p}$ disappears from $\hat{A}_1^{(B)}$.

Sensor behavior. Rather than providing the composite solution for the fields ψ and χ throughout the eIPMC domain, we opt to characterize the eIPMC sensor behavior by calculating the eIPMC current output (per unit nominal surface area) associated to the mechanical deformation and the electrochemical response. To this aim, first, we calculate the charge storage at the electrodes as the jump of the electric displacement at the polymer-metal interfaces, that is, $\hat{q} = \hat{\psi}'(0) = -\hat{\psi}'(2)$, see also [10]. Specializing this expression at the grounded electrode, we have $\hat{q} = \hat{C}_2^{(G)}$. From Eq. (7), it is thus evident that the eIPMC current, being equal to the time derivative of the charge, is given by $\hat{A}_1^{(B)}$ so that, in summary

$$\hat{I} = \frac{s}{2(s+1)}\hat{V} + \frac{s\gamma}{2(s+1)}\hat{p} = Y(s)\hat{V} + G(s)\hat{p}, \tag{11}$$

with obvious meaning of the symbols $Y(s)$ and $G(s)$. Equation (11) is thus our main modeling results, demonstrating that the current output of the eIPMC depends through an admittance on the voltage across its electrodes, and the mechanical deformation behaves as a voltage generator [10].

It is instructive to give Eq. (11) a physical interpretation in terms of an equivalent electric circuit with lumped parameters. Specifically, by dividing Eq. (11) through by $Y(s)$, and letting $Z(s) = 1/Y(s) = (2 + 2/s)$ as the impedance of the eIPMC,

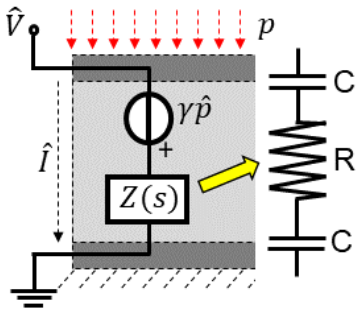

FIGURE 4. Equivalent lumped parameter circuit of the eIPMC compression sensor.

Eq. (11) becomes

$$\hat{V} = Z(s)\hat{I} - \gamma\hat{p}, \tag{12}$$

which represents the governing equation for the circuit in Fig. 4. It should be noted that the impedance $Z(s)$ of the eIPMC comprises the series arrangement of one resistor (of nondimensional resistance $\mathsf{R} = 2$) and two capacitors (each of nondimensional capacitance $\mathsf{C} = 1$) modeling diffusion through the bulk thickness of the polymer and capacitive effects due to charge double layers at the polymer-electrode interfaces, respectively.

We can thus distinguish two principal operating modes for the eIPMC compression sensor: the open circuit (OC) voltage sensing mode and the short circuit (SC) current sensing mode. In the OC voltage sensing mode, the circuit is open and therefore $\hat{I} = 0$. Thus, the voltage across the eIPMC electrodes upon application of normal pressure is given by

$$\hat{V}_{OC} = -\frac{G(s)}{Y(s)}\hat{p} = -\gamma\hat{p}. \tag{13}$$

Note that, at the timescale of the analysis of this paper, the eIPMC OC voltage output instantaneously follows the mechanical input. This is consistent with what observed for example in [9]. Importantly, if no mechanical asymmetry is present in the eIPMC, $\gamma = 0$ and no voltage is observed upon application of the mechanical pressure, see also [22]. Conversely, in the SC current sensing mode, the electrodes of the eIPMC are shorted and therefore $\hat{V} = 0$. Thus, the current through the eIPMC upon application of normal pressure is given by

$$\hat{I}_{SC} = G(s)\hat{p} = \frac{s\gamma}{2(s+1)}\hat{p}. \tag{14}$$

Note that, differently from the OC voltage, the SC current response depends on the rate of change of the applied pressure (via the term $s\hat{p}$) and its dynamics is mediated by the time constant of the RC equivalent circuit. It is illustrative to consider the response to a step input pressure, for which $\hat{p} = p_0/s$, with p_0 the magnitude of the step input. In this case, the nondimensional time domain response of the current is given by $I_{SC}(t) = (\gamma p_0/2)\mathrm{e}^{-t}$. Once again, if no mechanical asymmetry is present in the eIPMC, no current transient is observed upon application of the mechanical pressure. These modeling results will be examined in the context of mechanical compression sensing experiments performed on eIPMCs in the next section.

EXPERIMENTS, RESULTS, AND DISCUSSION

Experiments were conducted to compare the measured normalized open-circuit voltage between standard (control) IPMC sensors fabricated from Nafion polymer sheets to eIPMCs fabricated using two approaches: (1) filament-based fused-deposition manufacturing (FDM 3D printing) and (2) inkjet printing. The FDM 3D-printed samples consisted of macro-scale surface features and the inkjet printing process created micro-scale surface features. The details of the eIPMC fabrication processes and the measured results are described below. Figure 5 and 6 show the FDM 3D printer and samples considered in this study.

eIPMC Fabrication

The control IPMC sensors were fabricated from commercially-available Nafion sheet stock (Ion Power, Inc., membrane N117) using standard techniques for plating platinum electrodes as described in [31]. The control sensors have smooth surfaces, and one is shown in Fig. 5(c) with thickness of approximately 200 μm. The sizes of the control samples where approximately 9.5 mm $\times$ 31 mm and 12.5 mm $\times$ 15 mm. Color codes in Fig. 5(c) are to facilitate book-keeping with the presentation of the results in the following.

The FDM 3D-printed eIPMC samples were created using the FDM technique described in [5], where a LulzBotTAZ6 3D printer was modified to print the custom-made Nafion precursor filament. Figure 5(a) shows the 3D printer, and Fig. 5(b) shows an illustration of the basic structure of 3D-printed eIPMC sensors with 3D-printed polymer membrane sandwiched between two platinum metal electrodes. The 3D-printing process to create the eIPMC samples first starts with creating a solid computer model with desired features. Next, the solid model is sent to the 3D printer to print the desired shape of the eIPMC sensor using ionomeric precursor filament material, layer by layer. Afterwards, the manufactured precursor structure is chemically "activated" [5]. This process involves hydrolyzing the precursor filament in an aqueous solution of potassium hydroxide (KOH) and dimethyl sulfoxide (DMSO, C_2H_6OS). Afterwards, multiple layers (up to 3) of platinum material is deposited on the surface of the printed membrane to create electrodes through an electroless plating process. The two-point resistance method was employed to check for sufficient conductivity of the electrode surface. Two eIPMC samples each with different surface textures were created as shown in Fig. 5(c).

Sample eIPMC sensors with microfeatures in the form of

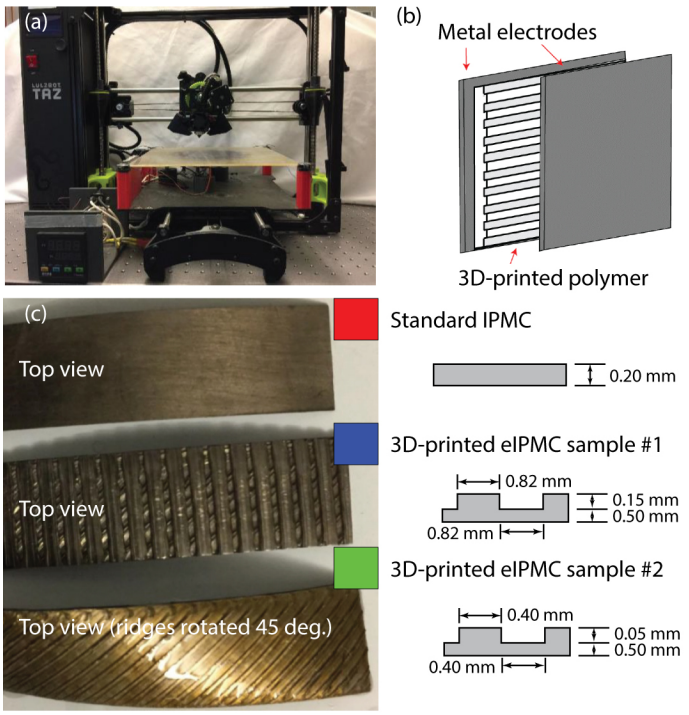

FIGURE 5. Sample eIPMCs fabricated using FDM 3D printing process: (a) custom-designed 3D IPMC printer; (b) basic structure of 3D-printed eIPMC sensor with 3D-printed polymer membrane sandwiched between two platinum metal electrodes; and (c) three types samples and dimensions of features created for testing.

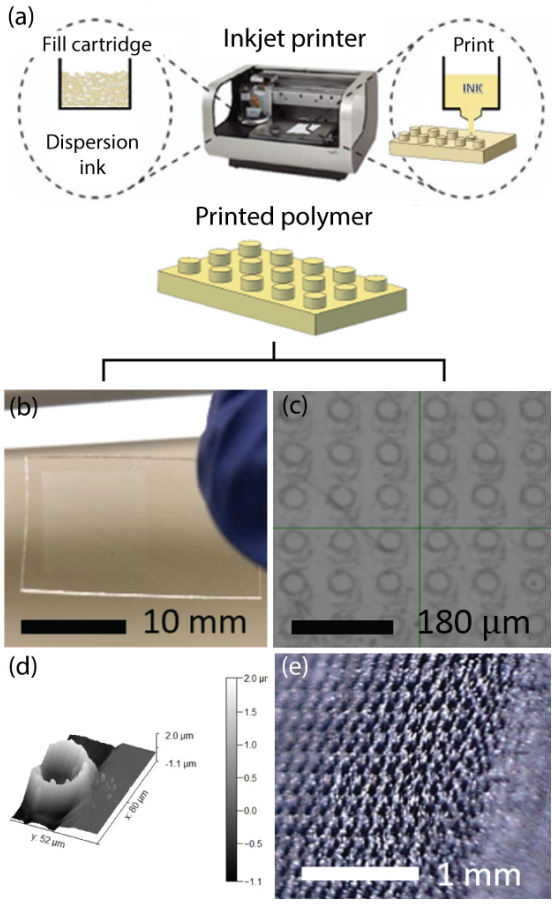

FIGURE 6. Sample eIPMCs fabricated using inkjet printing technology: (a) inkjet printing process; (b) Nafion membrane with features printed onto the surface using an inkjet printer; (c) close-up view of the printed Nafion dots with spacing between 87-92 μm and dot diameter between 43-51 μm and height of approximately 2 μm; (d) AFM image of printed dot showing approximate dimensions; and (e) close-up view of plated surface of eIPMC

micrometer-scale dots were created on the surface of a Nafion sheet stock. The eIPMC microfeatures were printed on the N117 Nafion Membrane from a FUJIFILM DMP-2850 Dimatix Materials Inkjet Printer using a specially designed ink consisting of 5% weight D521 alcohol-based Nafion dispersion and propyl alcohol, see Figure 6(a). The ink concentration of 1:19 (v/v) was optimized based on the required surface tension (28–42 dynes/cm) and viscosity (10–12 cP) parameters of the 1 pL and 10 pL print cartridges. Before printing, the Nafion substrate was tightly secured to an acrylic plate using 3M adhesive tape and placed inside the printer chamber. The microfeature droplets were then deposited using a custom print file that controlled the droplet formation from the piezoelectric cartridge nozzles by adjusting the nozzle voltage, jetting frequency, and waveform program. Multiple passes were employed to achieve the desired height of the microfeatures in a layer-by-layer fashion.

Figure 6(b) shows a sample of the Nafion membrane with printed micro-scale dots. Close-up view of the dots are shown in Fig. 6(c), where Nafion dots with spacing between 87-92 μm, dot diameter between 43-51 μm, and height of approximately 2 μm. Figures 6(d) and (e) show an AFM image of a printed dot and a close-up view of the plated surface, respectively.

After printing, the eIPMC Nafion membrane was plated with platinum metal electrodes using the sample process described for the control and FDM 3D-printed samples. Importantly, from Fig. 6(e), it can be seen that the microfeatures are preserved after the electroding process.

Sensor Characterization Apparatus

The sensor characterization apparatus shown in Fig. 7(a) is used to apply pressure to IPMC sensors and to measure the open-circuit voltage response. The apparatus consists of a stepper motor that is controlled to actuate a plate to apply pressure. A load cell measures the load for pressure control. The experimental configuration for the FDM 3D-printed and inkjet printed eIPMCs voltage sensing test are shown in Fig. 7(b).

Prior to testing, each sample is fully hydrated in DI water. The step load is applied to the eIPMC sensor and held until decompression is initiated after 30 seconds. The total duration of each test is 60 seconds and the open circuit voltage and the mechanical step response are recorded for each sample.

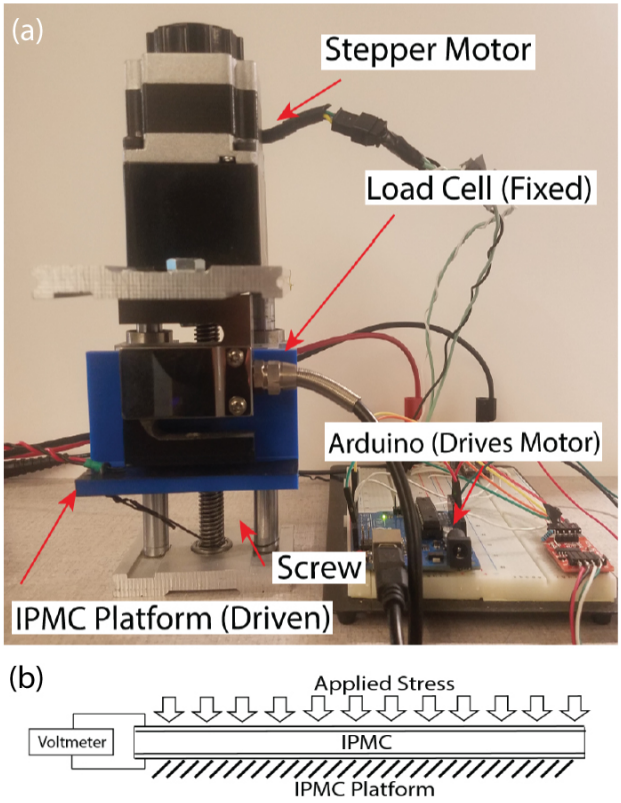

FIGURE 7. (a) Experimental setup for measuring open-circuit voltage of fabricated IPMC and eIPMC samples. (b) Experimental configuration for measuring open-circuit voltage of test samples.

Results and Discussion

The results for the measured normalized open-circuit voltage, $\hat{V}_{OC}$, plotted against the normalized applied pressure, $\hat{p}$, for the IPMC sensors are shown in Fig. 8. All test presented here are averages of multiple repetitions and concerned with the steady-state response of the system to be compared with the modeling results in Eq. (13). As in the model above, the open circuit voltage is normalized by the thermal voltage $V_{\text{th}} = RT/F \approx 25.4\,\text{mV}$ at room temperature, and the pressure is normalized by the polymer Young's modulus $E_p = 150\,\text{MPa}$, see for example [32].

As the results show in Fig. 8(a), the enhancement in sensing voltage is readily apparent between the control and eIPMC sensors. In particular, the results for the FDM 3D-printed eIPMC sensors show that the open circuit voltage increases with increased pressure. The trend is entirely consistent with the proposed model and Eq. (13), which predicts a linear increase. Through curve fit, the open circuit voltage vs. pressure slope for the 3D-printed eIPMC sample 1 and 2 is 72.66 and 149.56, respectively. The voltage output of the standard IPMC is significantly smaller for any value of the applied pressure and does not display a clear trend. A few comments are in order to interpret these results in terms of the modeling contributions of the previous section. The presence of macroscale ridges such as the ones in Fig. 5 is expected to significantly modify the strain field that would develop in a conventional IPMC and create inhomogeneous strain through the thickness, as for example shown in Fig. 2. However, it should be noted that, differently from the representative case studied above via finite element analysis, the dimension $\tilde{d}$ of the ridges is very large with respect to the polymer semithickness, that is, $\tilde{d} = 0.6$ for the 3D-printed eIPMC sample 1 and $\tilde{d} = 0.2$ for the 3D-printed eIPMC sample 2. As such, two important differences arise from our simplified minimal mechanical and chemoelectromechanical model: (1) the dilatation field may be significantly affected in a region sufficiently far from the engineered electrode and (2) important chemoelectromechanical phenomena can actually occur within the polymer protrusion regions of the engineered electrode. These changes would call for at least a 2D fully coupled chemoelectromechanical analysis of the system which is significantly more complicated than our approach which aims at distilling the fundamental aspects of the problem. Furthermore, additional and possibly important effects that we have neglected (e.g. steric effects, composite layers, electrode surface roughness, chemoelectromechanical nonlinearities, non-rigid electrodes) may play a role in the response. Even though we don't hope to capture the correct value of γ from our minimal model, it is remarkable that a fairly linear behavior is observed, consistently with what has been predicted. It is more difficult to correlate the voltage vs. pressure slope to the geometrical aspects of the interface. We predict that the more asymmetry is produced in the dilation at the electrodes, the higher the voltage response will be for a given pressure. The qualitative difference between the response of sample 1 and 2 could be explained by noticing that the ridges in sample 2 have shorter wavelength and smaller amplitude than those in sample 1. For small applied pressure, especially given the fact that the eIPMC samples are compressed between parallel plates, the sample 2 eIPMC would contract in an almost homogeneous fashion, not too dissimilar from the control sample. Larger wavelength and larger amplitudes of the ridge would instead cause significant asymmetry in the sample 1 eIPMC. Vice versa, for large values of the pressure, the polymer deformation could possibly better follow the shape of the (non-rigid) electrode and yield an enhanced voltage output. The existence of a possibly critical pressure, for the geometry under study, is evidenced by the jump around $\hat{p} = 0.8 \times 10^{-4}$. Finally, the response of the control sample should be identically null, according to Eq. (13). However, small, uncontrollable differences between the electrode morphology cause mechanical asymmetry and a non-zero, albeit erratic, response.

Likewise, the same basic trend is observed for the inkjet printed samples compared to the control sample, where the the slope for the inkjet printed sample is approximately 117.71. Importantly, note that the control sample in Fig. 8(b) is different than the control sample in Fig. 8(a), as explained below. Results in Fig. 8(b) show, on the other hand, that the response of the control sample is inconclusive. It should be remarked that, in order to minimize as much as possible the impact of the electrode fabrication on the performance of control IPMC and microscale inkjet printed eIPMC, the control and the eIPMC sample are si-

multaneously fabricated from a single Nafion membrane, which is only patterned in part as in Fig. 6(b), and is cut to separate the control and the eIPMC sample after the electroding process. Given the particular shape of the polymer protrusions resulting from the inkjet printing process (see Fig. 6(d)), the actual deformation process upon application of the pressure may differ significantly from the minimal model of our finite element analysis. Nevertheless, the response of the inkjet printed eIPMC is consistently higher than the control experiments, on the order of +50%–150%. A "jump" similar to the case of sample 2 in Fig. 8(a) can be observed in the neighborhood of $\hat{p} = 1.2 \times 10^{-4}$, suggesting that the experimental compression conditions may be dependent on the actual value of the applied pressure.

These results on open circuit voltage response for compression sensing in eIPMCs are the first of their kind and show the potential for enhanced sensing capabilities through engineered interfaces. Remarkably, the minimal model proposed captures the essence of the structure-property relationships to demonstrate enhanced strain sensing performance. One last comment should be briefly directed to the comparison of the control response in Figs. 8(a) and (b), the latter being almost an order of magnitude larger than the former. The only evident explanation for this behavior can be once again ascribed to asymmetry caused by uncontrollable electrode surface roughness. Note here that the Nafion membrane in the control sample of Fig. 8 was not sandblasted before plating [18] to preserve the inkjet printed microfeatures. This is yet another datapoint corroborating the huge variability in IPMC behavior dependent on uncontrollable fabrication conditions. We hope that 3D-printing and advanced manufacturing technicques of ionomer membranes with engineered properties will alleviate this problem in the future.

CONCLUSIONS

In this paper, we described the design of tailored 3D-structured (engineered) polymer-metal interfaces to create enhanced ionic polymer-metal composite (eIPMC) sensors with superior performance. Differently than traditional IPMC benders, these sensors are designed for operation in compression mode. A physics-based chemoelectromechanical model is developed to predict the performance of the eIPMC sensor. The model incorporates structure microfeature effects, including microscale feature thickness, size, and spacing, that are translated into a dilatation, or volume change, in response to applied mechanical pressure. The dilatation is thus used as input in an analytically tractable chemoelectromechanical model that captures the essential physics of the problem and provides insight into the behavior of the sensor under open circuit and short circuit conditions. Two novel approaches were described to create functional samples of eIPMC sensors using fused deposition manufacturing and inkjet printing technologies. Experimental results were presented to show enhancement in compression sensing capabilities compared to traditional sensors fabricated from sheet-form IPMC material and the effectiveness of the minimal model to interpret and explain the observed sensor behavior.

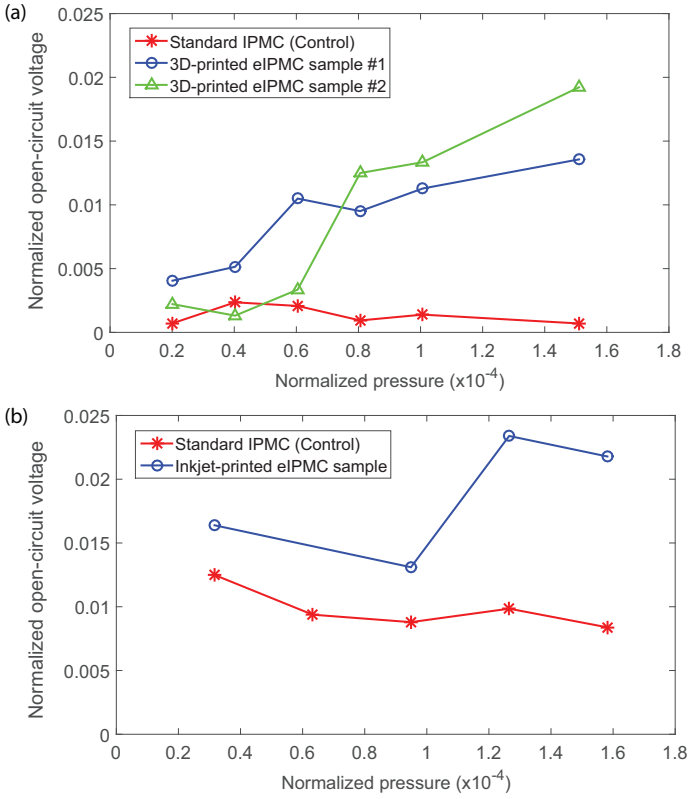

FIGURE 8. Measured normalized open-circuit voltage, $\hat{V}$, plotted against the normalized applied pressure, $\hat{p}$, for (a) FDM 3D-printed eIPMC sensors and (b) inkjet printed eIPMC sensor.

ACKNOWLEDGMENTS

This research was supported, in part, by the National Science Foundation under grants 1809852, 1809455, and 1545857. Rebecca Histed is supported by a National Science Foundation Graduate Research Fellowship Program grant number 1937966. Chantel Lapins is supported through the REU program associated with NSF grant number 1830958. Any opinions, findings, and conclusions or recommendations expressed in this material are those of the authors and do not necessarily reflect the views of the sponsor.

REFERENCES

[1] Shahinpoor, M., ed., 2015. *Ionic Polymer Metal Composites (IPMCs): Smart Multi-functional Materials and Artificial Muscles*. Royal Society of Chemistry.

[2] Oguro, K., Asaka, K., and Takenaka, H., 1993. US Patent 5,268,082: actuator element.

[3] Shahinpoor, M., Adolf, D., Segalman, D., and Witkowski, W., 1993. US Patent 5,250,167: Electrically controlled polymeric gel actuators.

[4] Shahinpoor, M., and Mojarrad, M., 2000. US Patent 6,109,852: Soft actuators and artificial muscles.

[5] Carrico, J. D., Traeden, N. W., Aureli, M., and Leang,

K. K., 2015. "Fused filament 3D printing of ionic polymer-metal composites (IPMCs)". *Smart Mater. Struct.,* **24**(12), p. 125021 (11 pages).

[6] Patel, S., Park, H., Bonato, P., Chan, L., and Rodgers, M., 2012. "A review of wearable sensors and systems with application in rehabilitation. journal of neuroengineering and rehabilitation". *Journal of neuroengineering and rehabilitation,* **9**(1), p. 21.

[7] Amjadi, M., Kyung, K.-U., Park, I., and Sitti, M., 2016. "Stretchable, skin-mountable, and wearable strain sensors and their potential applications: A review". *Advanced Functional Materials,* **26**(11), pp. 1678–1698.

[8] Safari, A., and Akdogan, E. K., eds., 2008. *Piezoelectric and Acoustic Materials for Transducer Applications*, 1 ed. Springer, New York, NY.

[9] Aureli, M., and Porfiri, M., 2013. "Nonlinear sensing of ionic polymer metal composites". *Continuum Mechanics and Thermodynamics,* **25**(2), pp. 273–310.

[10] Aureli, M., Prince, C., Porfiri, M., and Peterson, S. D., 2010. "Energy harvesting from base excitation of ionic polymer metal composites in fluid environments". *Smart Materials and Structures,* **19**(1), p. 015003.

[11] Farinholt, K., and Leo, D. J., 2004. "Modelling of electromechanical charge sensing in ionic polymer transducers". *Mechanics of Materials,* **36**(5), pp. 421–433.

[12] Biddiss, E., and Chau, T., 2006. "Electroactive polymeric sensors in hand prostheses: Bending response of an ionic polymer metal composite". *Medical Engineering and Physics,* **28**(6), pp. 568 – 578.

[13] Pugal, D., Jung, K., Aabloo, A., and Kim, K. J., 2010. "Ionic polymer–metal composite mechanoelectrical transduction: review and perspectives". *Polymer International,* **59**(3), pp. 279 – 289.

[14] Bahramzadeh, Y., and Shahinpoor, M., 2011. "Dynamic curvature sensing employing ionic-polymer-metal composite sensors". *Smart Materials and Structures,* **20**(9), p. 094011.

[15] Farinholt, K. M., Pedrazas, N. A., Schluneker, D. M., Burt, D. W., and Farrar, C. R., 2009. "An energy harvesting comparison of piezoelectric and ionically conductive polymers". *Journal of Intelligent Material Systems and Structures,* **20**(5), pp. 633–642.

[16] Giacomello, A., and Porfiri, M., 2011. "Underwater energy harvesting from a heavy flag hosting ionic polymer metal composites". *Journal of Applied Physics,* **109**(8), p. 084903.

[17] Cha, Y., Verotti, M., Walcott, H., Peterson, S. D., and Porfiri, M., 2013. "Energy harvesting from the tail beating of a carangiform swimmer using ionic polymer metal composites". *Bioinspiration & Biomimetics,* **8**(3), p. 036003.

[18] Aureli, M., Lin, W., and Porfiri, M., 2009. "On the capacitance-boost of ionic polymer metal composites due to electroless plating: Theory and experiments". *Journal of Applied Physics,* **105**(10), p. 104911.

[19] Zangrilli, U., and Weiland, L. M., 2011. "Prediction of the ionic polymer transducer sensing of shear loading". *Smart Materials and Structures,* **20**(9), p. 094013.

[20] Kocer, B., Zangrilli, U., Akle, B., and Weiland, L., 2015. "Experimental and theoretical investigation of ionic polymer transducers in shear sensing". *Journal of Intelligent Material Systems and Structures,* **15**, pp. 2042–2054.

[21] Kocer, B., 2014. "Experimental study of ionic polymer metal transducers characterization of transient response in sensing". Ph.D. Thesis, University of Pittsburgh, Swanson School of Engineering, USA.

[22] Volpini, V., Bardella, L., Rodella, A., Cha, Y., and Porfiri, M., 2017. "Modelling compression sensing in ionic polymer metal composites". *Smart Materials and Structures,* **26**(3), p. 035030.

[23] Porfiri, M., 2009. "Influence of electrode surface roughness and steric effects on the nonlinear electromechanical behavior of ionic polymer metal composites". *Physical Review E,* **79**(4), p. 041503.

[24] Cha, Y., Aureli, M., and Porfiri, M., 2012. "A physics-based model of the electrical impedance of ionic polymer metal composites". *Journal of Applied Physics,* **111**(12), p. 124901.

[25] Aureli, M., and Porfiri, M., 2012. "Effect of electrode surface roughness on the electrical impedance of ionic polymer metal composites". *Smart Materials and Structures,* **21**(10), p. 105030.

[26] Torquato, S., 2002. *Random Heterogenous Materials*. Springer, New York, US.

[27] Cha, Y., and Porfiri, M., 2014. "Mechanics and electrochemistry of ionic polymer metal composites". *Journal of the Mechanics and Physics of Solids,* **71**, pp. 156–178.

[28] Porfiri, M., 2019. "Sensing mechanical deformation via ionic polymer metal composites: a primer". *IEEE Instrumentation & Measurement Magazine,* **22**(5), pp. 5–12.

[29] Porfiri, M., 2008. "Charge dynamics in ionic polymer metal composites". *Journal of Applied Physics,* **104**(10), p. 104915.

[30] Nayfeh, A. H., 1981. *Introduction to Perturbation Techniques*. Wiley-Interscience, New York.

[31] Asaka, K., Kruusamae, K., Kim, K. J., Palmre, V., and Leang, K. K., 2016. *IPMCs as EAPs: how to start experimenting with them*. Springer International Publishing AG.

[32] Nemat-Nasser, S., and Wu, Y., 2003. "Comparative experimental study of ionic polymer-metal composites with different backbone ionomers and in various cation forms". *Journal of Applied Physics,* **93**(9), pp. 5255 – 5267.